Supplement of Weather Clim. Dynam., 6, 609–626, 2025
https://doi.org/10.5194/wcd-6-609-2025-supplement

Supplement of

Saharan warm-air intrusions in the western Mediterranean: identification, impacts on temperature extremes, and large-scale mechanisms

Pep Cos et al.

Correspondence to: Pep Cos (josep.cos@bsc.es)

Table S1. European Climate Assesment and Dataset (ECA&D) stations used to validate the extreme temperature link with Saharan warm air intrusions in Section 5.

Station name	Country	Latitude [º]	Longitude [º]	Height [m]
DROBETA TURNU SEVERIN	RO	44.63	22.63	77
LJUBLJANA BEZIGRAD	SI	46.07	14.51	299
ZARAGOZA AEROPUERTO	ES	41.66	-1.01	247
A CORUNA	ES	43.37	-8.42	58
SEVILLA/SAN PABLO	ES	37.42	-5.88	34
LEIPZIG-SCHKEUDITZ	DE	51.44	12.24	131
POITIERS - BIARD	FR	46.59	0.31	123
BASTIA	FR	42.54	9.49	10
MONTELIMAR	FR	44.58	4.73	73
ROTHAMSTED	GB	51.81	-0.36	128
SHANNON	IE	52.69	-8.92	6
STUTTGART/ECHTERDINGEN	DE	48.69	9.23	371
BARCELONA/AEROPUERTO	ES	41.29	2.07	4
STA. CRUZ DE TENERIFE	ES	28.46	-16.26	35
ESSEN-BREDENEY	DE	51.41	6.97	150
NEUSIEDL AM SEE	AT	47.95	16.83	117

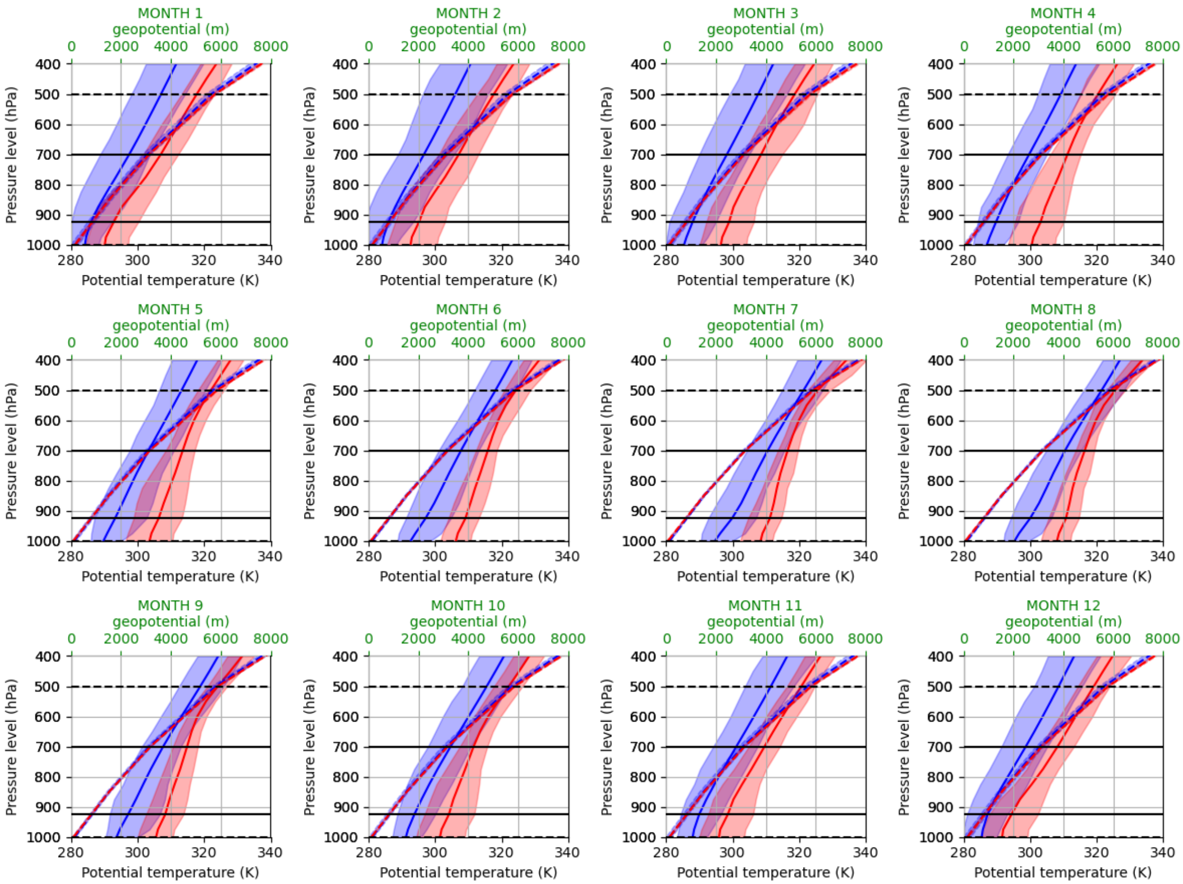

Figure S1. Monthly climatologies of vertical potential temperature (solid) and geopotential (dashed) profiles in the Mediterranean region (blue) and in the Sahara (red). The climatology of different months can be seen in the different panels. The shaded area is the interannual variability along the period 1981-2010.

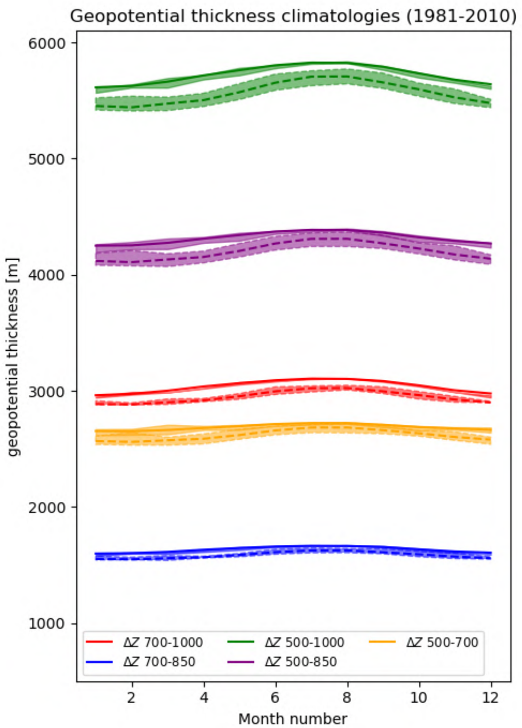

Figure S2. Climogram with monthly climatologies of geopotential thickness between different levels in the WMed (dashed) and in the Saharan (solid) regions. The shaded area is the interannual variability along the period 1981-2010.

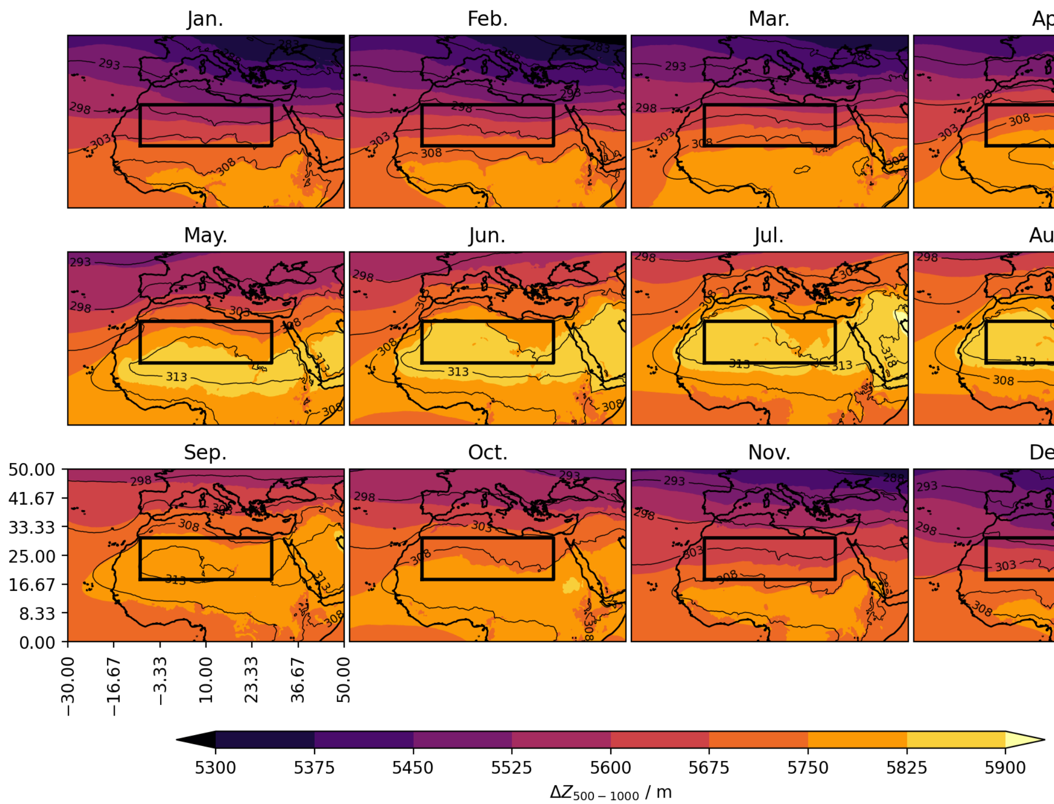

Figure S3. $\Delta Z_{500-1000}$ and $\overline{\theta}_{700-925}$ monthly climatologies during the period 1959-2022. The black box is the area of the Sahara desert (9ºW 29ºE 18ºN 30ºN) used as reference to compute the thresholds for the intrusion identification metrics.

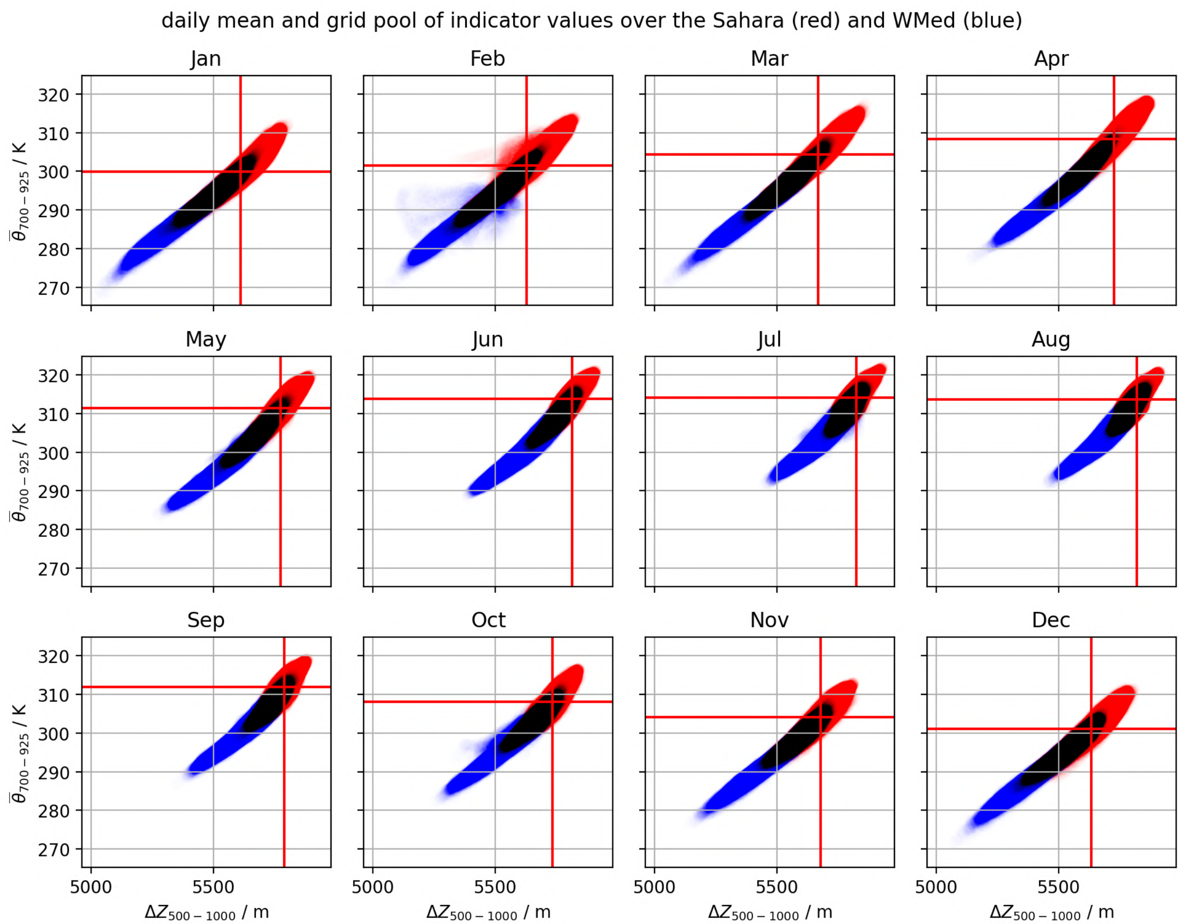

Figure S4. Monthly (different panels) pool of $\Delta Z_{500-1000}$ and $\overline{\theta}_{700-925}$ values over the whole grid points and days in the Western Mediterranean (blue) and the Sahara (red) regions for the period 1959-2022. The red lines show the Sahara climatologies. The black area shows overlap values between the Sahara and WMed.

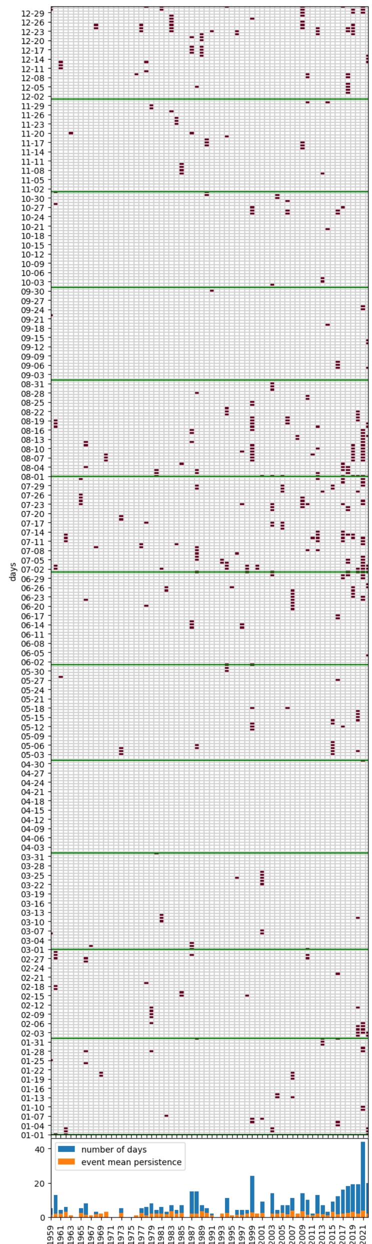

Figure S5. Historical catalogue of intrusion days in the period 1959-2022 (x-axis) and from the 1st of January to the 31st of December (y-axis). The days identified as intrusions are coloured in dark red. Green lines indicate the transition between months. The yearly number of intrusion days (blue) and the mean persistence (orange) are shown at the bottom.

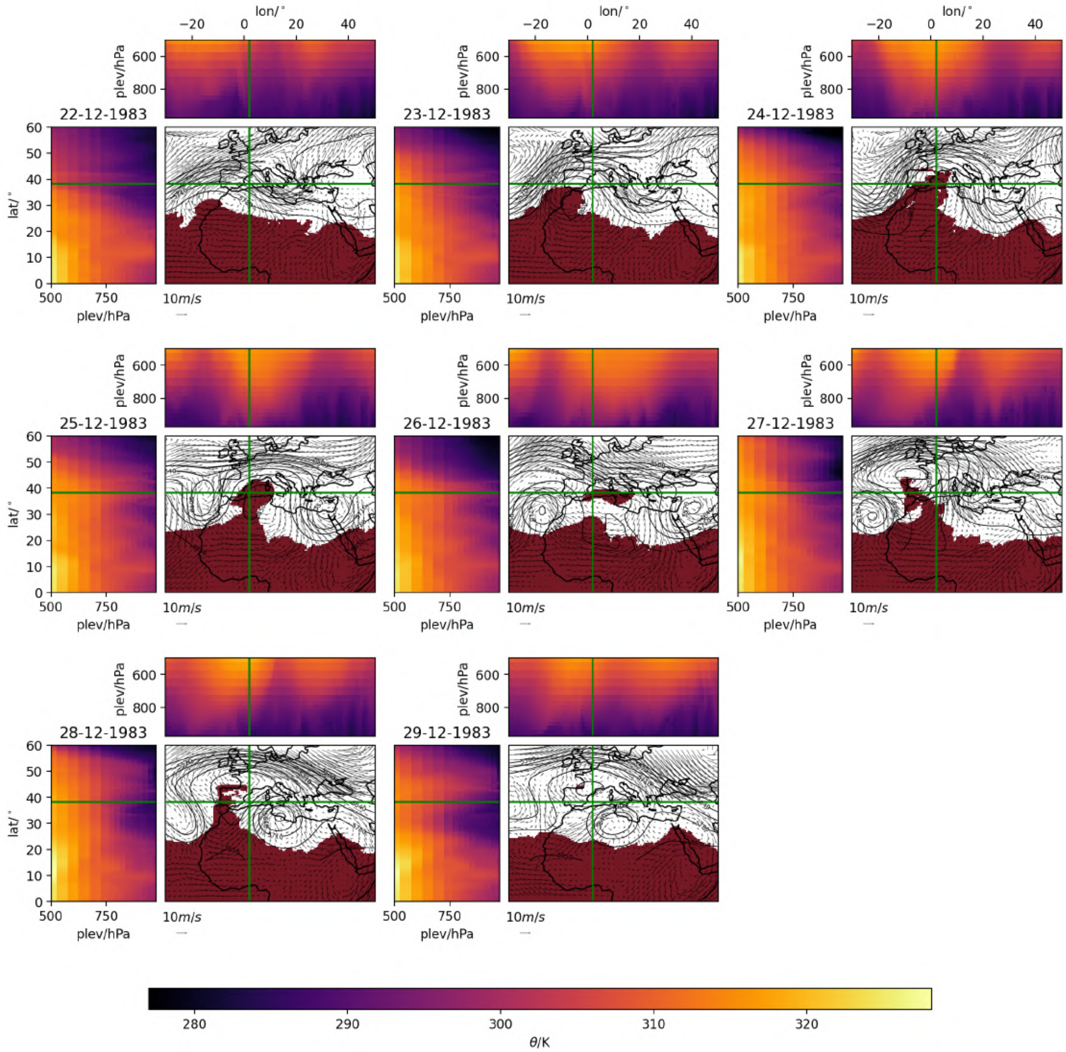

Figure S6. Same as Figure 3 but for the intrusion event observed in the period 23/12/1983 to 28/12/1983. The event is preceded by an intense trough developed in the North Atlantic that forces a subtropical ridge over the Western Mediterranean and the intensified northward winds in the western flank pushe a Saharan-like air mass (Saharan-like because red is present in all the longitudinal band below 25º N, even in the Atlantic) towards the Iberian Peninsula. The event is maintained by an omega block formed by a high pressure system over Europe (that ends up being a cutoff high), a low west of Iberia and a low over the Eastern Mediterranean. The vertical distribution of the potential temperature is also distinct and more homogeneous in the regions where the intrusion is present, but to a lesser extent than the summer event shown in Figure 3. At the end of the event, although the blocking persists, the air mass starts losing its properties. Note that the northward advection is briefly interrupted during the 26th of December and a Saharan air mass gets isolated over the Mediterranean, which is advected westward the next day and reconnected with the air masses in Africa thanks to the blocking.

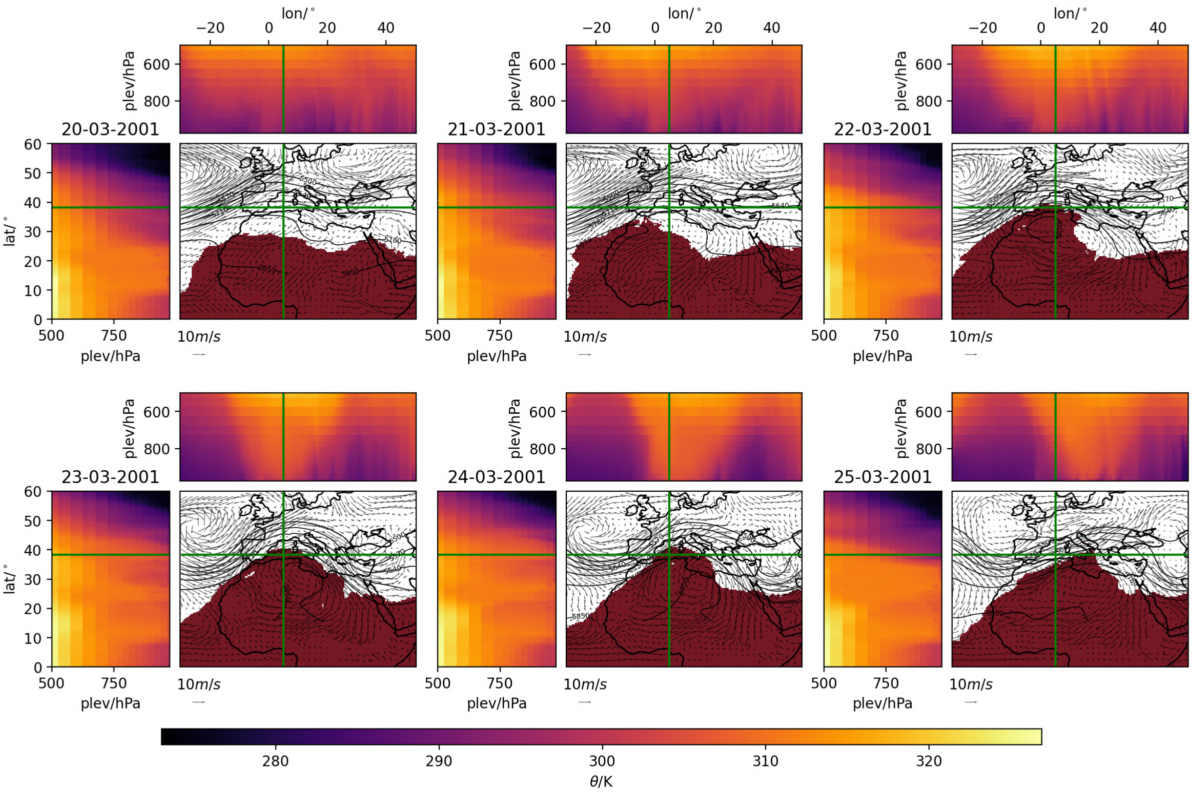

Figure S7. Same as Figure 3 but for the intrusion observed in the period 21/03/2001 to 24/03/2001. The event is preceded by a slight trough developed in the North Atlantic that forces a subtropical ridge over the Western Mediterranean and pushes a Saharan air mass towards the central WMed as the northward winds are intensified in the western flank of the ridge. In this case the intrusion propagates from West to East and from South to North and back South to Africa. The $\overline{\theta}_{700-925}$ vertical cross-sections show how the air mass is very warm and vertically homogeneous.

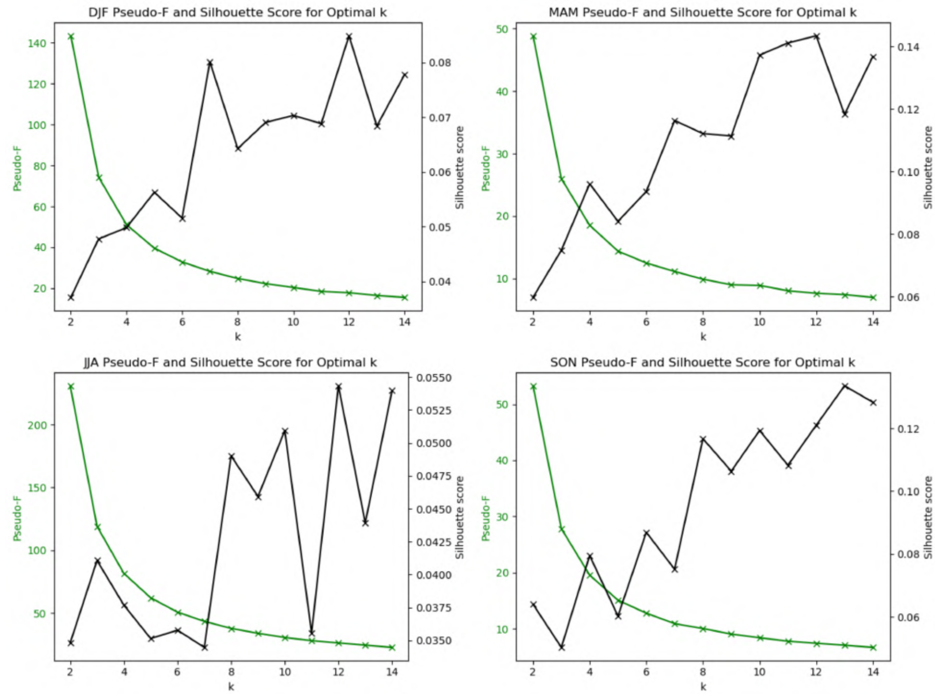

Figure S8. Silhouette (black) and Pseudo-F (green) scores as a function of the number of clusters for the DJF, MAM, JJA and SON seasons.

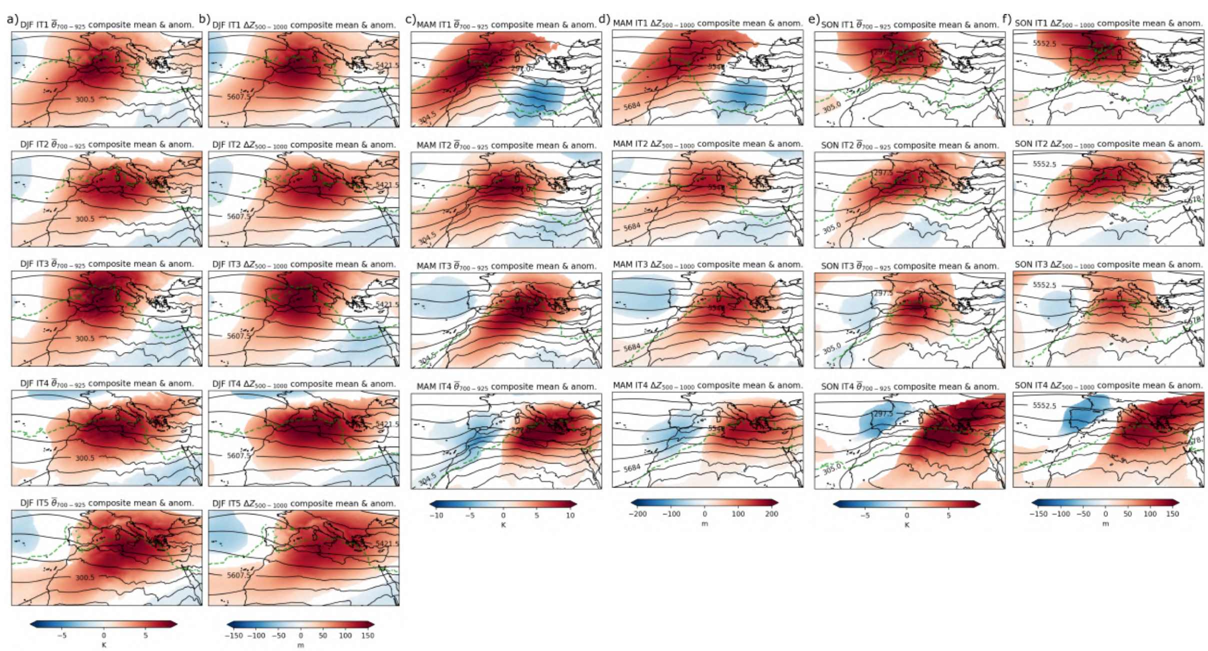

Figure S9. Same as Figure 4 but for DJF (a,b), MAM (c,d) and SON (e,f)

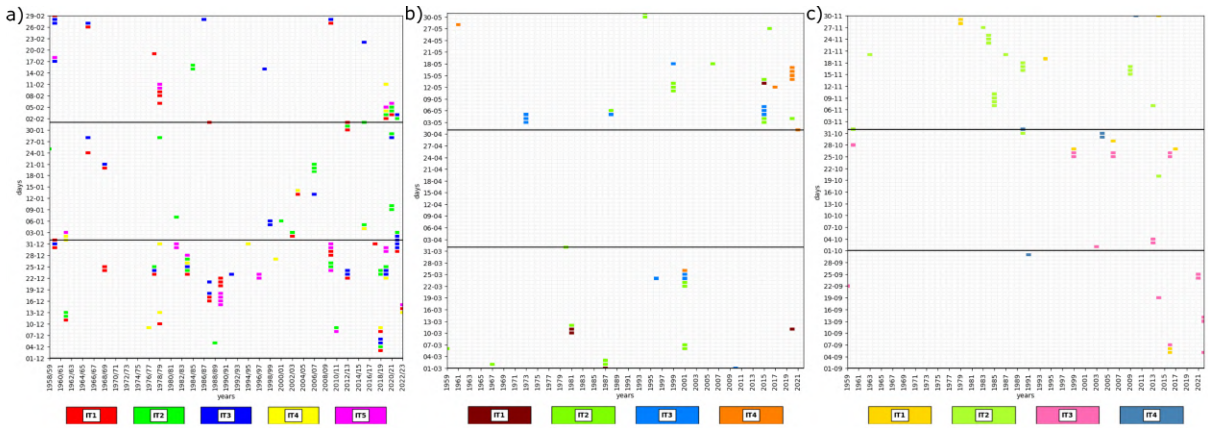

Figure S10. Same as Figure 5 but for a) DJF, b) MAM and d) SON.

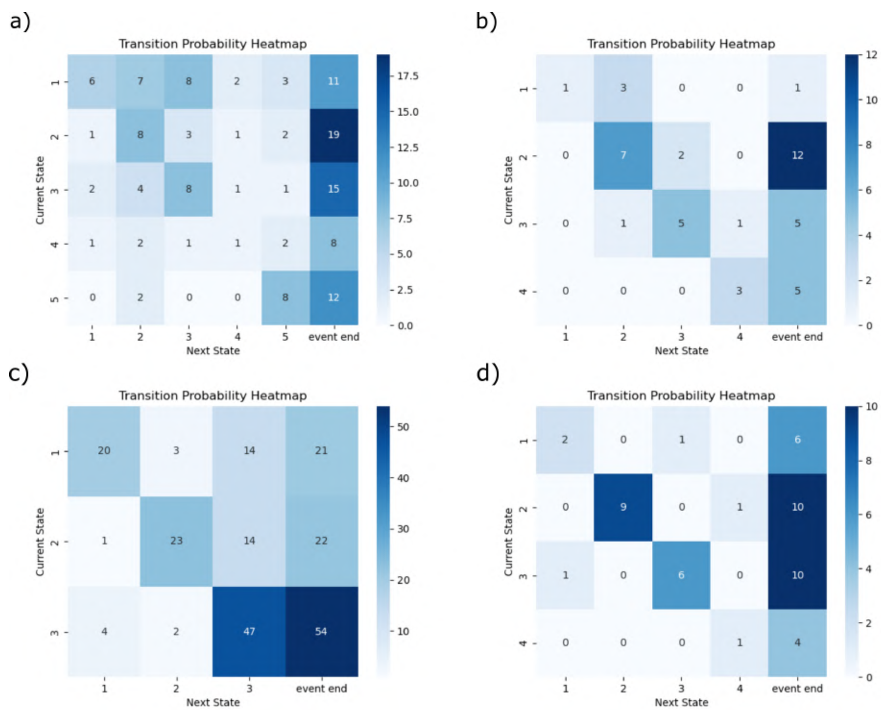

Figure S11. Transition probability heatmap showing the number of times that an intrusion day transitioned from one IT (current state) to another IT (next state) for a) DJF, b) MAM c) JJA d) SON. The next state axis has an extra column showing the amount of days that an intrusion event ended in a particular IT.

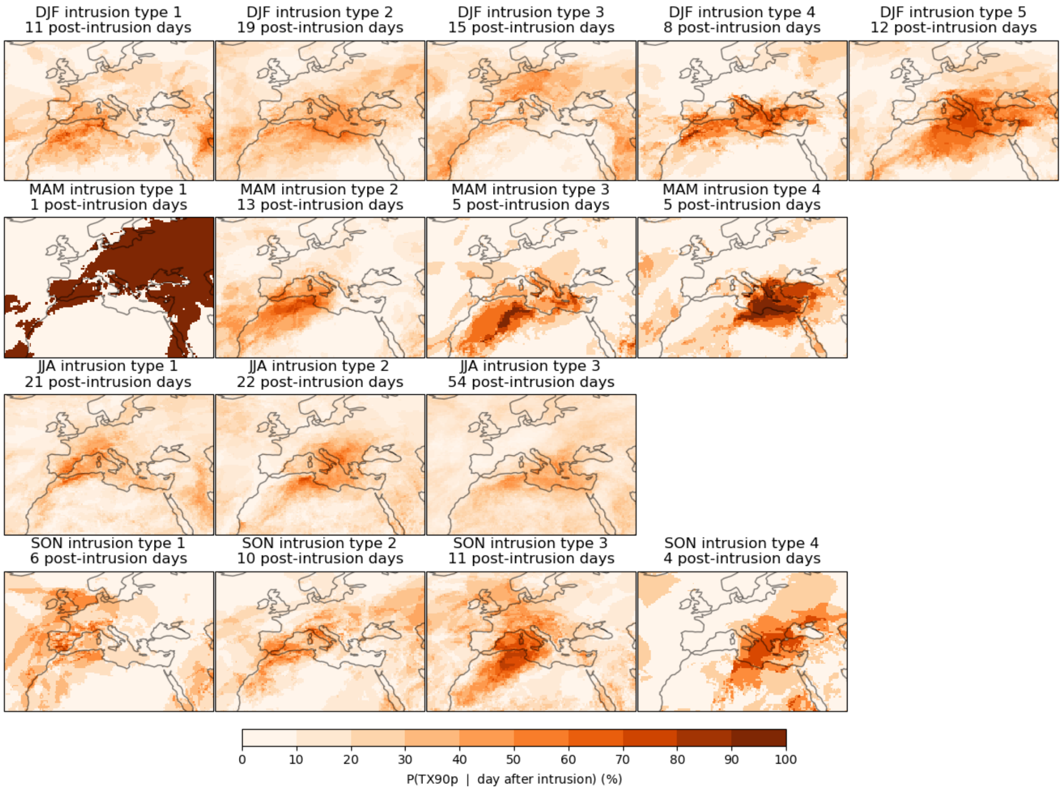

Figure S12. Impact of the days after an intrusion event on extreme temperatures in the EM region for the different seasons (rows) and ITs (columns). The impact is measured as the percentage of days after an intrusion event that coincide with an extreme temperature day (TX90p). The amount of days after an intrusion event for each season and IT is specified in the title of each panel (Note that MAM IT1 has only one day and hence the values can only be 100% or 0%).

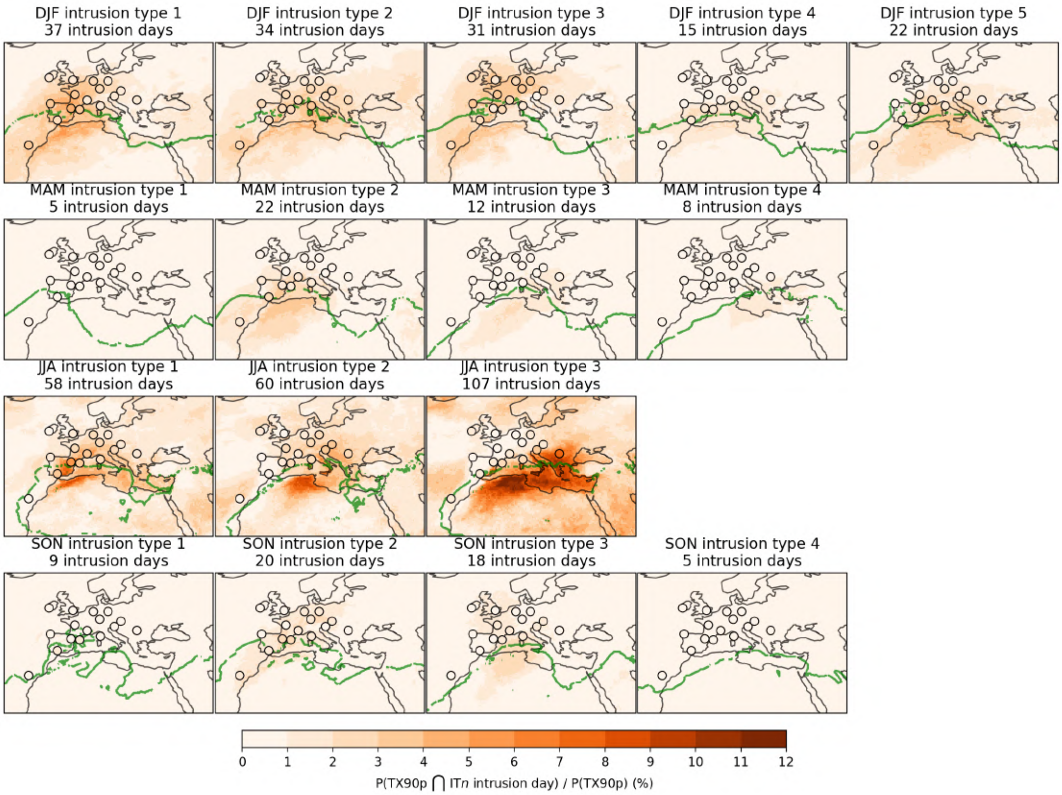

Figure S13. Contribution of the Saharan warm air intrusions to the extreme temperature days (TX90p) of each season (rows) and IT (columns). The contribution is calculated as the percentage of extreme temperature days that coincide with a Saharan intrusion.

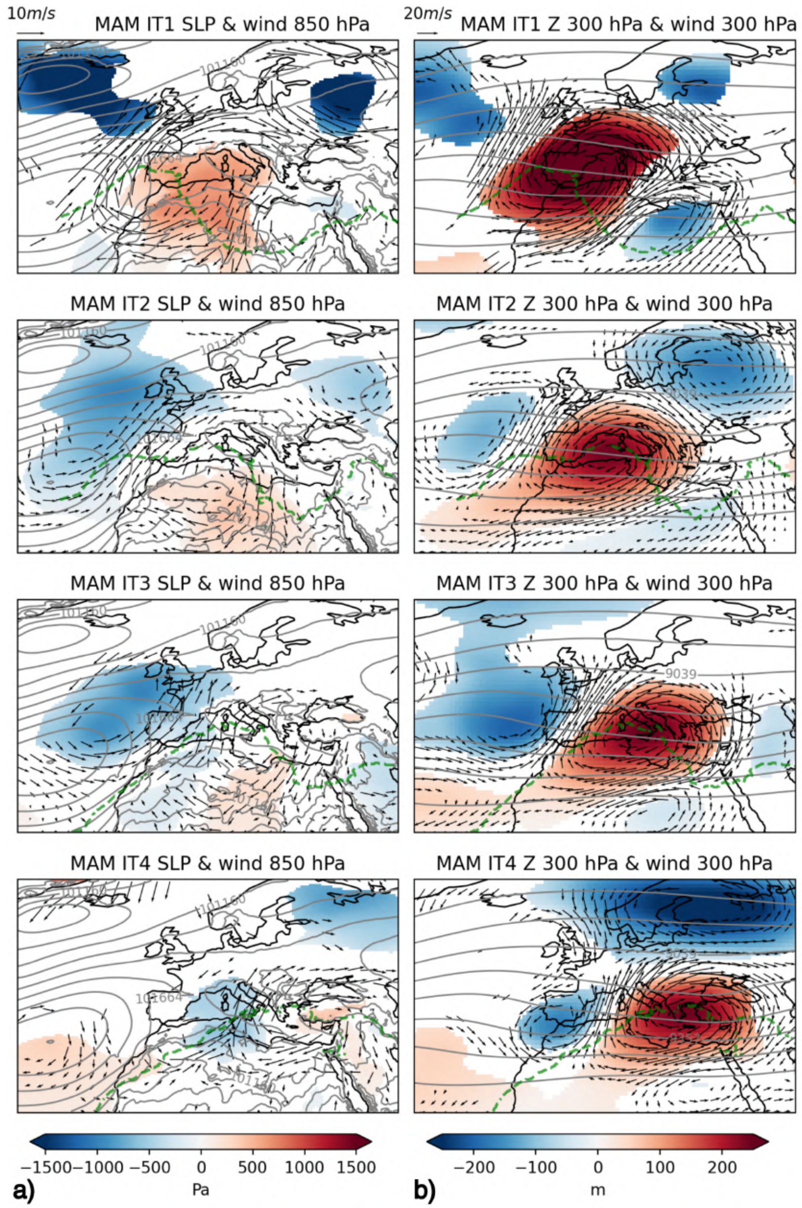

Figure S14. Same as Figure 7 but for the MAM ITs.

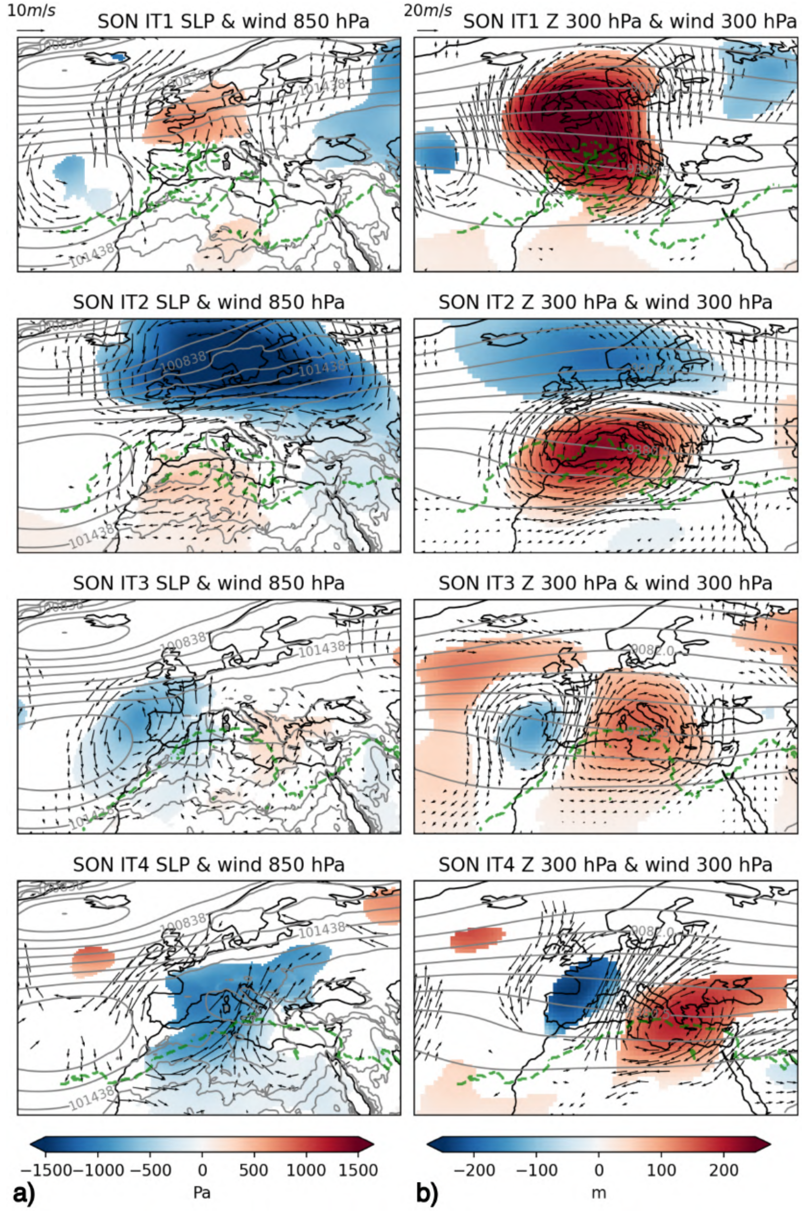

Figure S15. Same as Figure 7 but for the SON ITs.

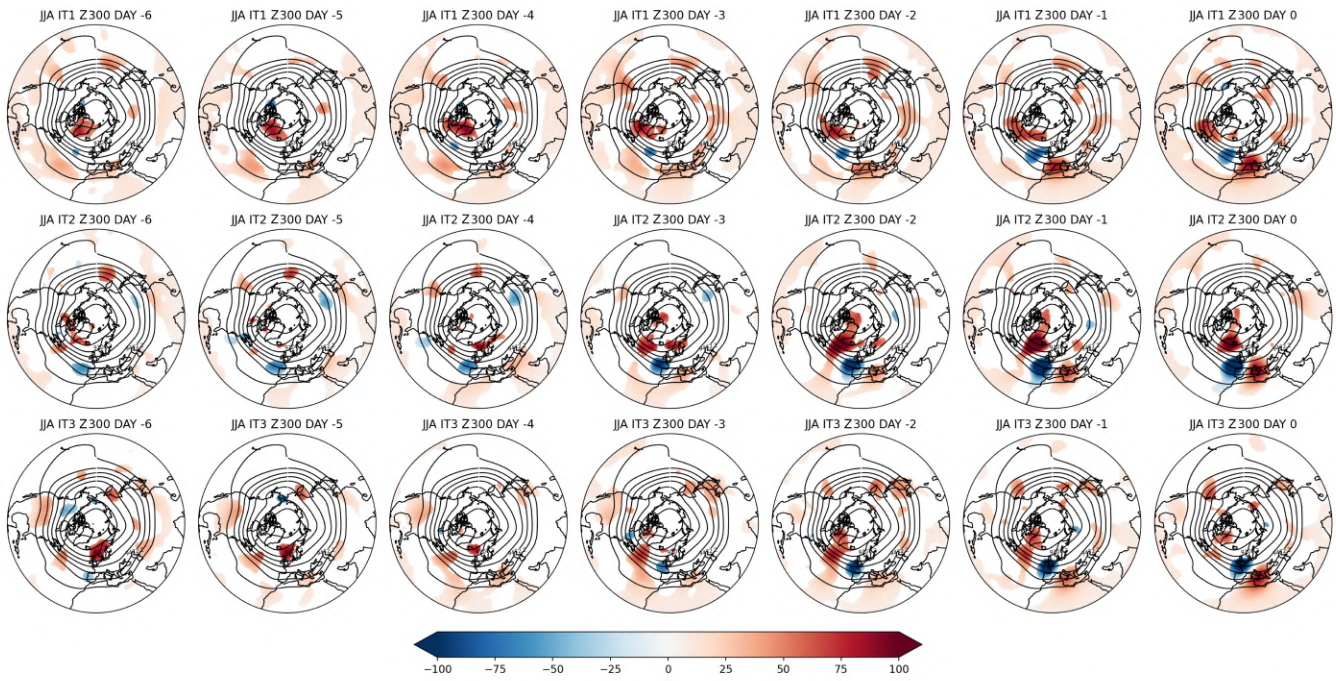

Figure S16. JJA composites of the first day (right) and the 6 days (right to left) prior to the intrusion events (columns) for geopotential height (shading) at 300 hPa for the three ITs (rows). Anomalies computed with respect to the non-intrusion climatologies of 7-day rolling windows centred on each calendar day between 1959-2022. Contours show the climatological 300 hPa geopotential height. No values are shown where the anomaly is not significantly different to 0 with a t-Student test and 95% confidence level.

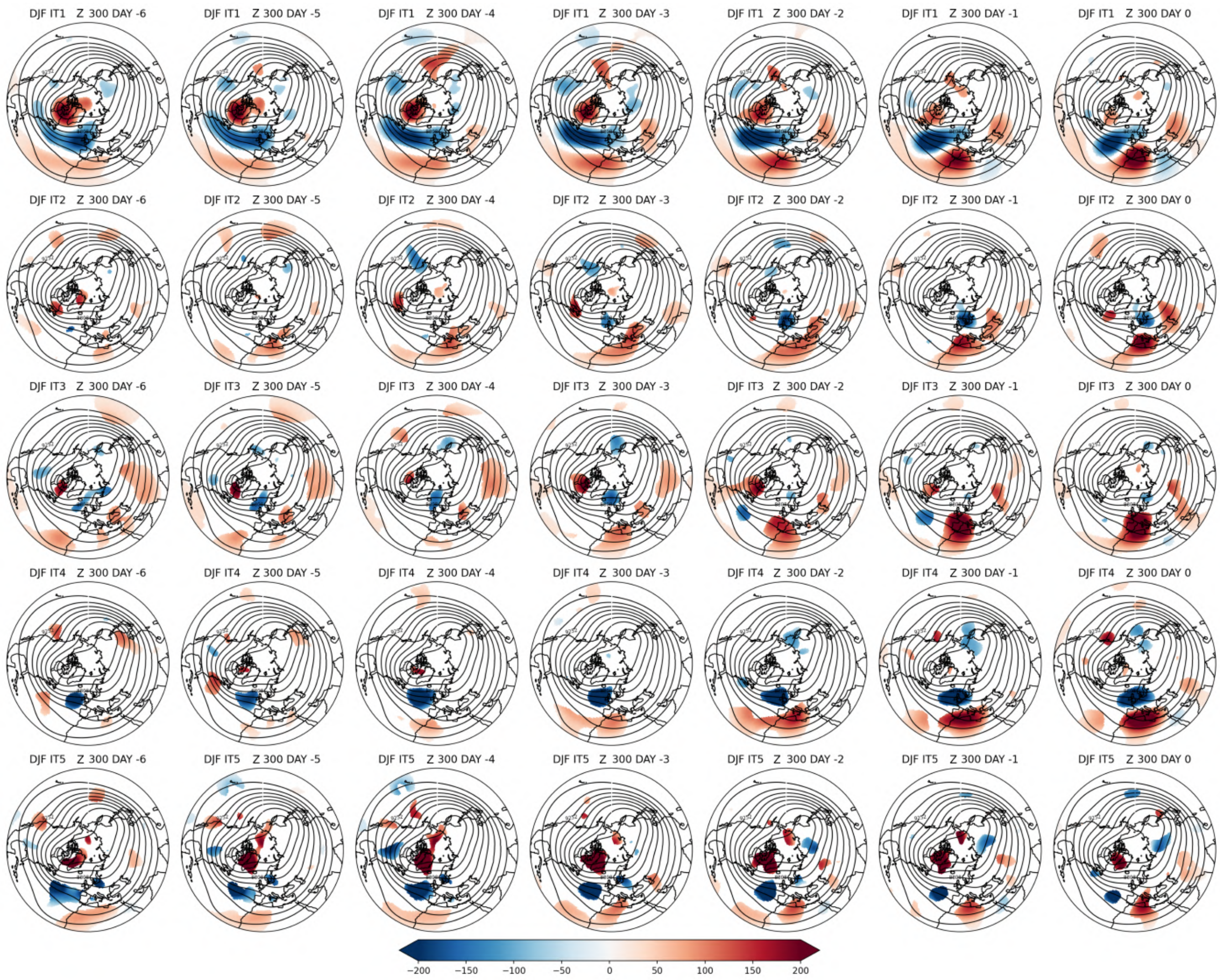

Figure S17. Same as S16 but for DJF